1. Title:

Prediction of Soot Formation Characteristics in a Pulverized-Coal Combustion Field by Large Eddy Simulations with the TDP Model

2. Authors:

H. Takahashi[a], N. Hashimoto[a*], H. Watanabe[b], R. Kurose[c], O. Fujita[a]

[a]*Division of Mechanical and Space Engineering, Hokkaido University, Kita13 Nishi8, Kita-ku, Sapporo, Hokkaido 060-8628, Japan*

[b]*Department of Mechanical Engineering, Kyushu University, 744 Motooka, Nishi-ku, Fukuoka 819-0395, Japan*

[c]*Department of Mechanical Engineering and Science, Kyoto University, Kyoto daigaku-Katsura, Nishikyo-ku, Kyoto 615-8540, Japan*

3. * Corresponding Author. E-mail address: nozomu.hashimoto@eng.hokudai.ac.jp

4. Colloquium: SOLID FUEL COMBUSTION

5. Total length of paper and method of determination: **6137 words** (Method 1)

, excluding title block, abstract, and separate list of figure captions.

6. Equivalent lengths:

1) Main text: 2852 words
2) References: 554 words
3) Figures with caption: 1949 words

Fig. 1: (64 mm + 10 mm) × (2.2 words/mm) + 2 words = 164

Fig. 2: (46 mm + 10 mm) × (2.2 words/mm) + 20 words = 143

Fig. 3: (58 mm + 10 mm) × (2.2 words/mm) + 11 words = 160

Fig. 4: (89 mm + 10 mm) × (2.2 words/mm) + 22 words = 239

Fig. 5: (85 mm + 10 mm) × (2.2 words/mm) + 9 words = 218

Fig. 6: (144 mm + 10 mm) × (2.2 words/mm) × 2 column + 59 words = 736

Fig. 7: (38 mm + 10 mm) × (2.2 words/mm) + 12 words = 117

Fig. 8: (64 mm + 10 mm) × (2.2 words/mm) + 10 words = 172

4) Tables: 394 words

Table 1 : (5 text lines + 2 blank) × 7.6 words/line × 2 columns = 106

Table 2 : (13 text lines + 2 blank) × 7.6 words/line = 114

Table 3 : (8 text lines + 2 blank) × 7.6 words/line = 76

Table 4 : (11 text lines + 2 blank) × 7.6 words/line = 98

5) Equations: 388 words

Abstract

In this study, the soot formation characteristics in a pulverized-coal combustion field formed by a 4 kW Central Research Institute of Electric Power Industry (CRIEPI) jet burner were predicted by large eddy simulation (LES) employing a tabulated-devolatilization-process model (TDP model) [N. Hashimoto et al., Combust. Flame 159 (2012) 353-366]. This model enables to take into account the effect of coal particle heating rate on coal pyrolysis. The coal-derived soot formation model proposed by Brown and Fletcher [A. L. Brown and T. H. Fletcher, Energy Fuels 12 (1998) 745-757] was employed in the LES. A comparison between the data predicted by LES and the soot volume fraction distribution data measured by laser induced incandescence confirmed that the soot formation characteristics in the coal combustion field of the CRIEPI burner can be accurately predicted by LES. A detailed analysis of the data predicted by LES showed that the soot particle distribution in this burner is narrow because the net soot formation rate is negative on both sides of the base of the soot volume fraction. At these positions, soot particles diffused from the peak position of soot volume fraction are oxidized due to a relatively high oxygen concentration. Finally, the effect of soot radiation on the predicted gas temperature distribution was examined by comparing the simulation results obtained with and without soot radiation. This comparison showed that the maximum gas temperature predicted by the simulation performed with soot radiation was over 100 K lower than that predicted by the simulation performed without soot radiation. From result strongly suggests the importance of considering a soot formation model for performing numerical simulations of a pulverized-coal combustion filed.

Keywords:

1) Soot formation; 2) Coal combustion; 3) LES; 4) TDP model; 5) Numerical simulation

List of figures

Fig. 1 Computational domain.

Fig. 2 Comparison between the calculated coal particle distributions with coal particle temperature and a direct photograph of a pulverized-coal jet flame.

Fig. 3 Selection probability of coal particle heating rate for each particle diameter.

Fig. 4 Radial distribution of the time-averaged axial velocity of coal particles at (a) HAB = 60 mm and (b) HAB = 120 mm.

Fig. 5 Comparison between measured [1] and calculated soot volume fraction.

Fig. 6 Comparison between the radial distributions for (a), (b) the soot LII signal [2] and the calculated soot volume fraction, (c), (d) the Mie scattering signal [2] and the calculated surfaces area of coal particles, and (e), (f) the calculated gas temperature and the O_2 concentration, and (g), (h) the net soot formation rate, at HAB=60 and 120 mm, respectively.

Fig. 7 Mean soot particle diameter as a function of the height above burner.

Fig. 8 Effect of soot radiation on the ensemble-averaged gas temperature distribution.

1. Introduction

Coal-fired thermal power plants generate over 40% of the total electricity that is produced worldwide, and pulverized-coal combustion is used in the majority of them. Coal, as fuel, is expected to continue being a major source of energy in the future owing to its abundance and wide distribution. From this viewpoint, to achieve a more sustainable society and processes with improved efficiency, it is of high interest to reduce air pollution in coal-fired thermal power plants. To attain this, understanding the gas flow patterns, temperature distribution, distribution of chemical species concentration, and the behaviour of coal particles in furnaces is very important. Numerical simulations can be a useful tool to understand such phenomena in furnaces, and various models and simulation techniques for pulverized-coal combustion fields have been developed. On the other hand, validation data are necessary for the development of new models and simulation techniques. Recently, various researchers have conducted numerical simulations of pulverized-coal combustion field formed by a small coal jet burner from the Central Research Institute of Electric Power Industry (CRIEPI) [1–4] for validation purposes. Several optical methods such as laser Doppler velocimetry and shadow Doppler particle analysis for particle velocity [3], planar laser-induced fluorescence (PLIF) for OH radicals [3], Mie scattering imaging for coal particle distribution [2,3], laser-induced incandescence (LII) for soot volume fraction [1,2], time-resolved laser induced incandescence (TiRe-LII) for primary soot particle diameter distribution [1], and simultaneous PLIF and LII for distributions of polycyclic aromatic hydrocarbons (PAHs) and soot particles [4], were applied to this burner. Using these experimental data, Reynolds averaged Navier-Stokes (RANS)-based simulations [5–8], large eddy simulations (LES) [9-15], and direct numerical simulations (DNS) [16-20] were conducted. However, for most of these simulations, soot particle formation was not considered despite the importance of soot particles as intermediate substances in the combustion process of volatile matter. Soot particles are also an important medium for radiative heat transfer. Recently, Xu et al. [8] conducted a RANS-based simulation with a soot formation model for CRIEPI burner and found that the effect of radiative heat transfer through soot particles was significant. However, no soot formation model has not been developed for LES. To the best of our knowledge, this is the first study that reports the characteristics of soot formation in a pulverized-coal combustion field predicted by LES. The purpose of this study is an establishment of soot formation model for LES of a turbulent coal flame and to investigate the effect of soot radiation on the temperature field of a turbulent coal flame.

In this study, the soot formation model proposed by Brown and Fletcher [21] was combined with a tabulated-devolatilization-process (TDP) model [22] and adapted to the LES performed for a pulverized-coal combustion

field. The accuracy of the soot formation model proposed by Brown and Fletcher was validated using data obtained by thermophoretic sampling in a laminar flow reactor [21]. In this study, validation of the soot formation model using two-dimensional data obtained by LII for the soot volume fraction distribution in a turbulent coal flame was conducted. Generally, most soot particles are considered to be generated from tar after the devolatilization of coal particles [21]. Therefore, a devolatilization model would play an important role in the prediction of soot formation. By employing TDP model [22], the effect of coal particle heating rate on devolatilization was considered. Numerical simulations were performed for the pulverized-coal combustion field formed by CRIEPI burner [1-3], and the simulation data were compared with the experimental data. Finally, the impact of radiative heat transfer on the temperature field was also examined.

2. Numerical models

2.1 Devolatilization model

In numerical simulations of the pulverized-coal combustion, the following equations for the devolatilization has been widely used:

$$dV/dt = K_v(V^* - V) \qquad (1)$$

$$K_v = A_v \exp\left(-E_v/R_u T_p\right), \qquad (2)$$

where $V^*$and V are the amount of volatile matter to be evolved and the amount of volatile matter which has already been evolved at a given time, respectively. A_v, E_v, R_u and T_p are the pre-exponential factor, activation energy, gas constant, and the coal particle's temperature, respectively.

In this study, a TDP model [22] was employed to consider the effect of particle heating rate on pyrolysis. The TDP model allows changing the parameters, V^*, A_v and E_v based on the heating rate of each particle. Those parameters are tabulated in the devolatilization database. In this study, the database produced by Hashimoto et al. [8] using software PC Coal Lab that can simulate the devolatilization process of coal with a FLASHCHAIN model [23], was adopted.

2.2 Soot model

In this study, soot was treated as a gas phase and its conservation equations are expressed as follows [24]:

$$\frac{\partial \rho_g \varphi}{\partial t} + \frac{\partial}{\partial x_j}\left(\rho_g u_j \varphi - \rho_g D_s \frac{\partial \varphi}{\partial x_j} - \gamma \frac{\mu}{T}\varphi \frac{\partial T}{\partial x_j}\right) = S_\varphi \,, \quad (3)$$

where φ is either N_C (number density of soot particles) or Y_C (soot mass fraction). D_s and γ are the soot diffusion coefficient and the coefficient for the thermophoretic force acting on the soot (expressed by Eq. (7)), respectively. D_s was calculated using following equation:

$$D_s = \mu/\sigma\rho_g \,, \quad (4)$$

where μ, σ and ρ_g are the viscosity of the gas, Schmidt number (= 700 [2]), and the gas density, respectively. S_{Y_C} (source term of Y_C) is expressed using the following equation:

$$S_{Y_C} = \rho_g(\dot{r}_{FC} - \dot{r}_{OC}), \quad (5)$$

where $\dot{r_{FC}}$ and $\dot{r_{OC}}$ are the soot formation and soot oxidation rates, respectively. S_{N_C} (source term of N_C) is expressed using the following equation:

$$S_{N_C} = \frac{\rho_g}{N_A}\left(\frac{N_A}{M_C \cdot C_{min}} \cdot \dot{r}_{FC} - \dot{r}_{AN}\right), \quad (6)$$

where $\dot{r}_{AN}$, M_C and C_{min} are the soot agglomeration rate, molecular weight of carbon, and the number of carbon atoms per incipient soot particle, respectively. In this study, C_{min} was set to 100, based on K. M. Leung et al. [25]. The term γ in Eq. (3) represents the thermophoretic transport, and is expressed by the following equation:

$$\gamma = \frac{3}{4\left(1 + \pi \cdot \frac{A}{8}\right)}, \quad (7)$$

where the accommodation coefficient A was set to 1.0 [26]. The soot formation rate from Eq. (5) is expressed using the following equation:

$$\dot{r}_{FC} = \rho_g \cdot \left(\sum_{i=1}^{4} \frac{Y_{s,Tar_i}}{MW_{Tar_i}} \right) \cdot A_{FC} \cdot e^{-\frac{E_{FC}}{RT}}, \quad (8)$$

where MW_{Tar_i}, A_{FC}, E_{FC} and R are the molecular weight of the tar species, the pre-exponential factor, the activation energy, and the gas constant (= 8.314 J/mol/K), respectively. Y_{S,Tar_i} (tar mass fraction) was calculated using the TDP model [22]. The soot oxidation rate in Eq. (5) is expressed by the following equation:

$$\dot{r}_{OC} = SA_{v,C} \cdot p_{O_2} \cdot T^{-\frac{1}{2}} \cdot A_{OC} \cdot e^{-\frac{E_{OC}}{RT}}, \quad (9)$$

where $SA_{v,C}$, and p_{O_2} represent the soot particle surface area per unit volume and the oxygen partial pressure, respectively. In this study, soot particles are assumed to be spherical, and $SA_{v,C}$ is expressed by the following equation:

$$SA_{v,C} = (\pi \cdot N_C)^{\frac{1}{3}} \cdot (6 \cdot Y_C)^{\frac{2}{3}} \cdot \rho_g \cdot \rho_C^{-\frac{2}{3}} \quad (10)$$

where ρ_C represents the soot particle density (= 1950 kg/m^3 [21]). The soot agglomeration rate in Eq. (6) is expressed using the following equation:

$$\dot{r}_{AN} = 2C_a \left(\frac{6M_C}{\pi \cdot \rho_C} \right)^{\frac{1}{6}} \left(\frac{6\kappa T}{\rho_C} \right)^{\frac{1}{2}} \cdot \left(\frac{\rho_g \cdot Y_C}{M_C} \right)^{\frac{1}{6}} (\rho_g \cdot N_C)^{\frac{11}{6}}, \quad (11)$$

where C_a is the collision frequency constant, which was assumed to be 3 [21]. This term is found in the Smoluchowski equation for the particle agglomeration rate, as described by Ulrich [27]. The values for the pre-exponential factor and the activation energy are listed in Table 1.

Table 1 transport equation source terms

Term	A	E	Ref.
$\dot{r_{FC}}$	5.02×10^{8} m^3·mol·s	198.9×10^{3} J·mol^{-1}	J. Ma [28]
$\dot{r}_{OC}$	1.09×10^{4} m^{-1}·s·kg^{-1}·$K^{-1/2}$	164.5×10^{3} J·mol^{-1}	Lee et al. [29]
$\dot{r}_{AN}$	N/A	N/A	Fairweather et al. [30]

2.3 Radiative heat transfer

In this study, the prediction of the radiative heat transfer was modeled using the discrete ordinate method [31] with the S4 approximation, which has 24 ordinate directions. The S4 approximation was selected to achieve accuracy and to save computational time.

The coal particles emissivity ϵ_p was set to 0.85, based on Kurose et al. [32]. The absorption coefficient k_a of the soot and gas mixture can be expressed using the following equation:

$$k_a = k_g + k_s \qquad (12)$$

where the gas absorption coefficient k_g was set to 0.075, and the soot absorption coefficient k_s was calculated using the following equation [33]:

$$k_s = 1.8644 \times 10^3 f_{v_{soot}} T, \quad (13)$$

where $f_{v_{soot}}$ is the soot volume fraction, and T is the gas temperature.

2.4 Motion of coal particles

Based on the motion equation for dispersed particles, the pulverized-coal particles were tracked in a Lagrangean manner. The char burning rate was calculated using the Field's model [34], which assumes that the char burning rate depends on both the chemical reaction and the diffusion rate of oxygen to the surface of the char particles. The interaction of conserved properties between the dispersed coal particle phase and gas phase was calculated using the particle-source-in cell (PSI-Cell) technique [35].

3. Numerical methods

The LES solver used in this study was the FrontFlow/Red developed by Numerical Flow Designing Co., Ltd. (NuFD). Dynamic Smagorinsky model was used as subgrid-scale (SGS) model. The SGS combustion model used was the scale similarity filtered reaction rate model (SSFRRM) [36] to consider the effect of SGS fluctuations on the filtered reaction rate by assuming that the largest of the SGSs are dynamically similar to the smallest of the resolved scales [37]. The use of SSFRRM model for a pulverized-coal combustion field was validated by Ahn et al. [14]. The generalized Favre filtered governing equation was solved for mass, momentum, species mass fraction and enthalpy.

The convective terms for momentum was approximated by combining 90% of a second-order central difference scheme with 10% of a first order upwind scheme. The convective terms for enthalpy and mass fractions were approximated by combining 50% of the second-order upwind scheme with 50% of the first-order upwind scheme. Time integration was performed using the Crank-Nicolson scheme.

Figure 1 shows the schematic view of the computational domain. The overall shape of the computational domain is a cylinder with a length of 560 mm (-60 < height above burner (HAB) < 500 mm) and a diameter of 200 mm. The location of burner exit was set to HAB=0 mm. The number of fluid cells and nodes was about 2.0 and 1.8 million. The calculation time step, Δt, was set at 2×10^{-5} s.

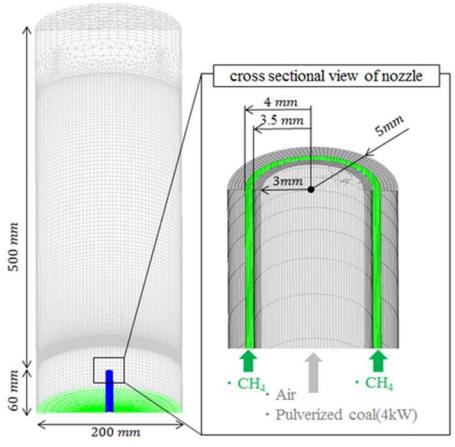

Fig. 1 Computational domain.

The simulation was performed based on the experimental conditions used by Hwang et al. [5]. Table 2 and 3 show the coal properties and experimental conditions. The air flow rate was set to 2.07×10^{-4} Nm^3/s, which is 0.27 Nm^3/s higher than the experimental value. This difference was introduced to account for the air that is

sucked by the coal feeder and added into the main flow [8]. The methane flow rate supplied from the external slit (0.5 mm) was set to 2.33×10^{-5} Nm^3/s. The air velocity around the burner nozzle was set at 1.5 m/s.

Table 2 Coal properties.

Proximate analysis	[wt%]
Moisture$^{\alpha}$	2.6
Ash$^{\beta}$	15.6
Volatile matter$^{\beta}$	26.9
Fixed carbon$^{\beta}$	57.9
Ultimate analysis	**[wt%]**
Carbon$^{\beta}$	71.9
Hydrogen$^{\beta}$	4.4
Oxygen$^{\beta}$	6.53
Nitrogen$^{\beta}$	1.5
Sulfur$^{\beta}$	0.39

α : as received basis, β : dry basis

Table 3 Experimental conditions

Coal feeding rate	1.49×10^{-4} kg/s
Air flow rate	1.80×10^{-4} Nm^3/s
Methane flow rate	2.33×10^{-5} Nm^3/s
Thermal input of methane	0.83 kW (LHV)
Thermal input of coal	4.19 kW (LHV)

Table 4 Initial diameter, mass fraction and feeding rate of pulverized-coal particles

Dia. [μm]	Mass Frac. [-]	Feeding Rate [kg/s]
5	6.76	1.01×10^{-5}
20	26.81	3.99×10^{-5}
40	24	3.58×10^{-5}
60	16.25	2.42×10^{-5}
80	12.2	1.82×10^{-5}
100	13.98	2.08×10^{-5}
		Total 1.49×10^{-4}

Table 4 shows the particle diameter distribution in the simulation. It was assumed that the pulverized-coal particles presented 6 different diameters. In addition, particles were classified according to their actual particle size distribution. The temperature and velocity of these particles in the inlet boundary were set to 298 K and 7.99 m/s, respectively, matching the experimental values.

4. Results and discussions

4.1 Flame shape

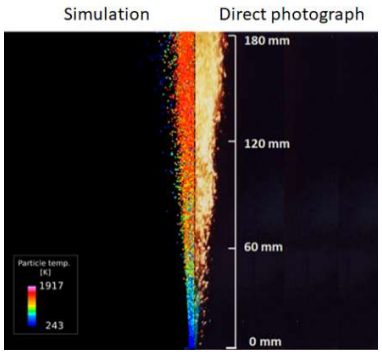

Fig. 2 Comparison between calculated coal particle distribution with coal particle temperature and direct photograph of pulverized-coal jet flame.

Figure 2 shows a comparison between the calculated coal particle distribution and a direct photograph of a pulverized-coal jet flame, as obtained by Hwang et al [3]. Based on this comparison, it was concluded that the calculated distribution of the coal particles with a high temperature is largely consistent with the luminous flame shape.

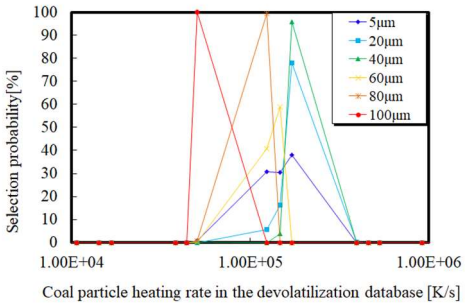

Fig. 3 Selection probability of particle heating rate for each coal particle diameter during calculation.

4.2 Coal particle velocity and calculated particle heating rate for each diameter

Figure 3 shows the probability density functions (PDFs) of the calculated heating rate for each particle diameter. It is found that the heating rate of smaller particles is higher than that of larger particles. This means that the ratio of volatile matter mass to coal particle mass for smaller particles is higher than that for larger particles. In other words, a larger amount of tar, which is the precursor of soot, is evolved from smaller particles.

Figure 4 (a) and (b) show the radial distribution of the time-averaged axial velocity of coal particles at HAB = 60 and 120 mm, respectively. These graphical representations indicate that for particle velocity, the calculated results are in good agreement with experimental results.

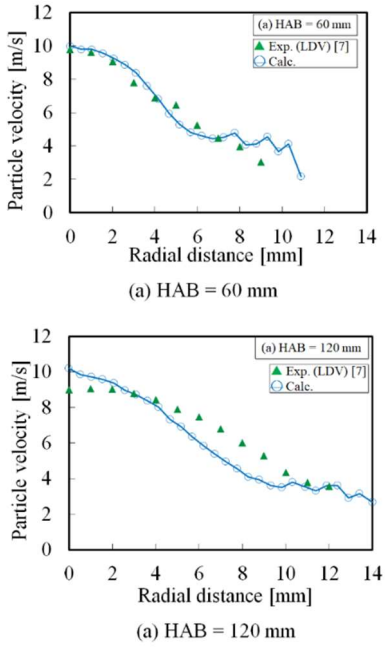

Fig. 4 Radial distribution of mean axial coal particle velocity at (a) HAB = 60mm and (b) HAB = 120 mm.

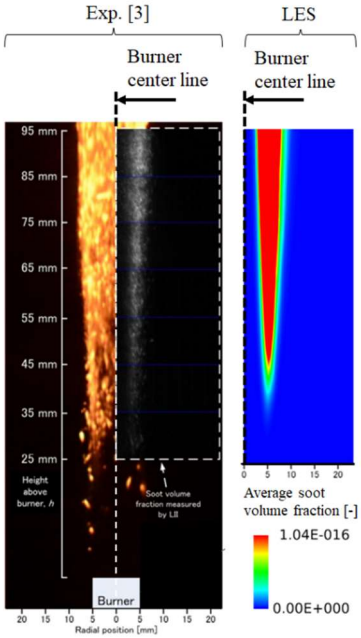

Fig. 5 Comparison between measured [1] and calculated soot volume fraction.

4.3 Detailed radial distributions of the soot volume fraction and the net soot formation rate

As shown in Fig. 5, the shape of calculated average soot volume fraction distribution was consistent with the shape of the distribution of the LII signal intensity, which is proportional to the soot volume fraction.

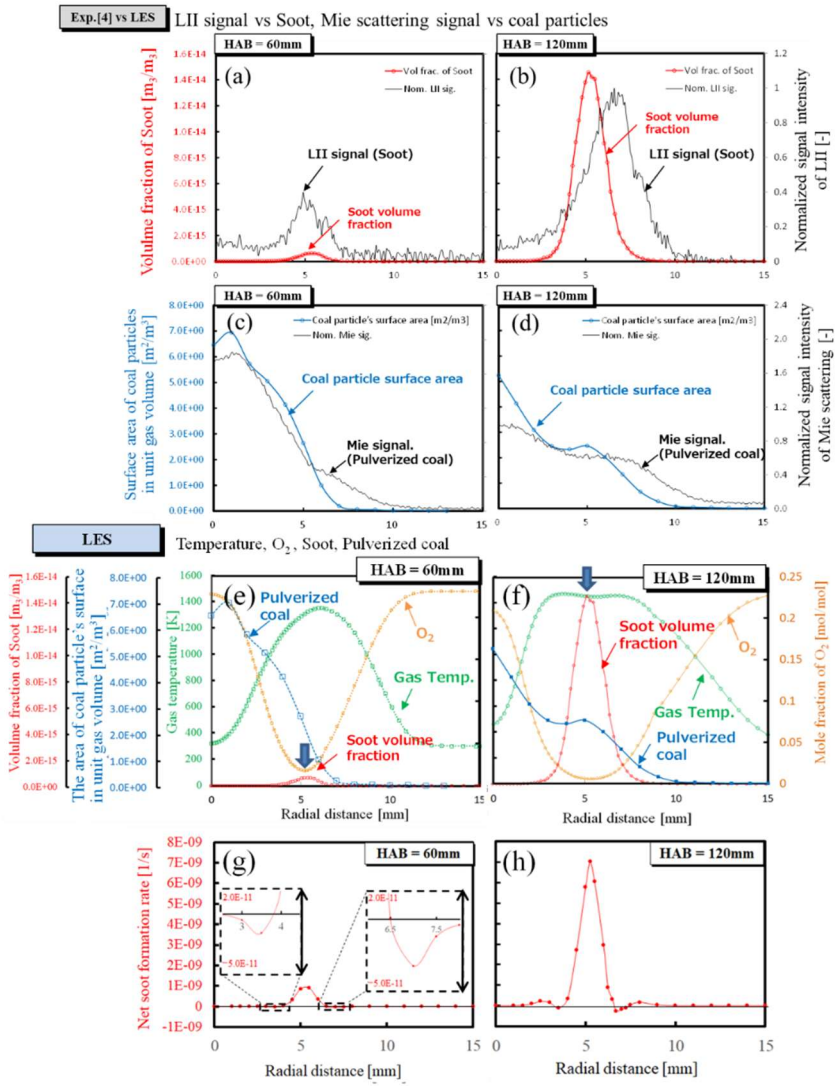

Fig. 6 Comparison of the radial distributions for (a), (b) the soot LII signal [2] and the calculated soot volume fraction, (c), (d) the Mie scattering signal [4] and the calculated surface area of coal particles, (e), (f) the calculated gas temperature and the O_2 concentration, and (g), (h) the net soot formation rate at a HAB=60 and 120 mm, respectively.

As shown in Fig. 6 (c) and (d), the Mie scattering signal distributions expand radially as the HAB increases. This tendency is well reproduced in the distributions of the calculated surface area of coal particles in the same graphs. Furthermore, the positions of the LII signal peak and the calculated soot volume fraction peak in Figs. 6 (a) and (b) are nearly the same. In addition, an expansion of the soot volume fraction distributions is also observed for both experimental and calculated data. In the calculated gas temperature and oxygen mass fraction distributions shown in Figs. 6 (e) and (f), it can be observed that at the position of the soot volume fraction peak the conditions of low oxygen concentration, high gas temperature, and presence of pulverized-coal particles are simultaneously met. This can be explained as follows: the positions of the net soot formation rate peak in Figs. 6 (g) and (h) match the positions of the soot volume fraction peak in Fig. 6 (e) and (f). The net soot formation rate distribution shows a negative net soot formation rate at both sides of the base of soot volume fraction peak, despite the soot volume fraction

steadily increasing at these positions as the HAB increases. This is due to the fact that the soot particles are diffused from the soot volume fraction peak toward both sides by a turbulence effect. At the positions where a negative net soot formation rate is observed, the oxygen concentration is higher than that in the positions of the soot volume fraction peak. This higher oxygen concentration leads to a higher soot oxidation rate. Even though the absolute value of the net negative formation rate is not that high, this position has a significant effect on the formation of a high soot volume fraction area. Although the graph is not shown in this paper due to space constraints, the soot formation and soot oxidation rates were much higher than the net soot formation (formation rate minus oxidation rate). The negative net soot formation rate is observed in those positions where the soot volume fraction is high enough. Basically, this means that in these positions, the soot particles are transported from the direction of the soot volume fraction peak, and no net soot is formed. This is the reason why the soot volume fraction exhibits a narrow distribution.

4.4 Mean soot particle diameter

Figure 7 shows the calculated mean soot particle diameter as a function of the HAB. The mean soot particle diameter, d_{mean}, was calculated by the following equation:

$$d_{mean}|_h = \frac{\sum_i (d_i \cdot N_{C_i} \cdot Y_{C_i})|_h}{\sum_i (N_{C_i} \cdot Y_{C_i})|_h}, \quad (14)$$

where d_i, N_{C_i} and Y_{C_i} are the ensemble-averaged soot diameter in cell i, number density in cell i, and soot mass fraction in cell i, respectively.

Figure 7 shows that the mean diameter increases with an increase in HAB. This tendency is consistent with the experimentally observed growth of primary soot particle diameter [1]. The absolute soot particle diameter values, shown in Fig. 7, are much smaller than the experimental values obtained by TiRe-LII (Ref. [1]). However, LII cannot detect the signal of very small soot particles, which explains this difference in absolute values for the calculated and the experimental data.

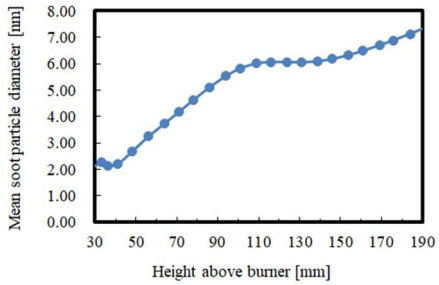

Fig. 7 Mean soot particle diameter as a function of height above burner.

4.5 Comparison of the gas temperature distributions with and without soot radiation

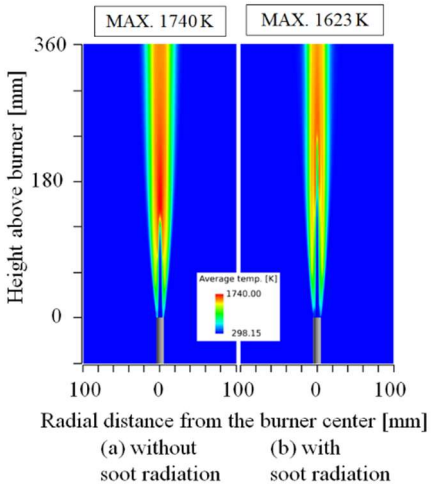

Fig. 8 Effect of soot radiation on the ensemble-averaged gas temperature distribution.

Figure 8 shows the calculated ensemble-averaged gas temperature distributions (a) without soot radiation and (b) with soot radiation. These results suggest that soot radiation causes a maximum gas temperature difference of over 100 K. Average heat flux at the outer boundary of the domain (100 mm from the burner center axis) with soot radiation was 2.95×10^{2} W/m^2, whereas without soot radiation it was 2.69×10^{-3} W/m^2. This large difference in heat flux causes a significant difference in the gas temperature. This result indicates the importance of a soot formation model in the numerical simulations of a pulverized-coal combustion field. If a soot formation model is not considered, the gas temperature can be significantly overestimated. Since gas temperature has significant effects on most phenomena related to the coal combustion fields, such as the devolatilization rate of coal particles, volatile matter reaction rate, surface reaction rate of char particles, and formation rate of pollutants such as NOx,

the soot formation model should be considered for an accurate prediction of a coal combustion field by numerical simulations.

5. Conclusions

In this study, LES of the coal combustion field of a 4 kW jet burner (CRIEPI burner) using a soot formation model with the TDP model was conducted. The predicted pulverized-coal particle velocity, the predicted soot volume fraction distributions, and growing tendency of the soot particles in the axial direction were in good agreement with experimatal data. The main findings from this study were the following:

(1) A detailed analysis of the data predicted by LES showed that soot particle distribution in this burner is narrow because the net soot formation rate is negative on both sides of the base of the soot volume fraction peak. The net soot formation rate is negative at these positions because soot particles diffused from the soot volume fraction peak are oxidized due to a relatively high oxygen concentration.

(2) Soot radiation significantly affects the prediction of gas temperature distribution in a pulverized-coal combustion field. Therefore, if a soot formation model is not considered, gas temperature can be overestimated. Since the gas temperature has significant effects on various phenomena in a pulverized-coal combustion field, it is very important to consider a soot formation model for performing the numerical simulation of a pulverized-coal combustion filed.

Acknowledgements

Part of this research was supported by JSPS KAKENHI Grant Number 15637712, and MEXT as "Priority issue on Post-K computer" (Accelerated Development of Innovative Clean Energy Systems).

References

[1] N. Hashimoto, J. Hayashi, N. Nakatsuka, K. Tainaka, S. Umemoto, H. Tsuji, F. Akamatsu, H. Watanabe, H. Makino, J. Therm. Sci. Technol. 11 (2016) 16-00387.

[2] J. Hayashi, N. Hashimoto, N. Nakatsuka, H. Tsuji, H. Watanabe, H. Makino, F. Akamatsu, Proc. Combust. Inst. 34 (2013) 2435–2443.

[3] S.M. Hwang, R. Kurose, F. Akamatsu, H. Tsuji, H. Makino, M. Katsuki, Energy Fuels 19 (2005) 382–392.

[4] J. Hayashi, N. Hashimoto, N. Nakatsuka, K. Tainaka, H. Tsuji, K. Tanno, H. Watanabe, H. Makino, F. Akamatsu, Proc. Combust. Inst., under review.

[5] J. Cai, M. Handa, M.F. Modest, Combust. Flame 162 (2015) 1550–1565.

[6] X.-Y. Zhao, D.C. Haworth, Combust. Flame 161 (2014) 1866–1882.

[7] K. Xu, Y. Wu, H. Shen, Q. Zhang, H. Zhang, Fuel 194 (2017) 297–305.

[8] N. Hashimoto, R. Kurose, H. Shirai, Fuel 97 (2012) 277–287.

[9] B.M. Franchetti, F. Cavallo Marincola, S. Navarro-Martineza, A.M. Kempf, Proc. Combust. Inst. 34 (2013) 2419–2426.

[10] O.T. Stein, G. Olenik, A. Kronenburg, F. Cavallo Marincola, B.M. Franchetti, A.M. Kempf, M. Ghiani, M. Vascellari, C. Hasse, Flow, Turbul. Combust. 90 (2013) 859–884.

[11] X. Wen, K. Luo, H. Jin, J. Fan, Combust. Theory Model. 21 (2017) 925–953.

[12] K. Wan, J. Xia, Z. Wang, M. Pourkashanian, K. Cen, Flow Turbul. Combust. 99 (2017) 531–550.

[13] X. Wen, Y. Luo, K. Luo, H. Jin, J. Fan, Fuel 188 (2017) 661–671.

[14] S. Ahn, K. Tanno, H. Watanabe, Appl. Therm. Eng. 124 (2017) 1194–1202.

[15] M. Rieth, A.G. Clements, M. Rabaçal, F. Proch, O.T. Stein, A.M. Kempf, Proc. Combust. Inst. 36 (2017) 2181–2189.

[16] Y. Bai, K. Luo, K. Qiu, J. Fan, Fuel 182 (2016) 944–957.

[17] T. Hara, M. Muto, T. Kitano, R. Kurose, S. Komori, Combust. Flame 162 (2015) 4391–4407.

[18] M. Muto, K. Tanno, R. Kurose, Fuel 184 (2016) 749–752.

[19] K. Luo, H. Wang, J. Fan, F. Yi, Energy Fuels 26 (2012) 6128-6136.

[20] M. Rieth, A.M. Kempf, A. Kronenburg, O. T. Stein, Fuel 212 (2018) 364-374.

[21] A.L. Brown, T.H. Fletcher, Energy Fuels 12 (1998) 745–757.

[22] N. Hashimoto, R. Kurose, S.-M. Hwang, H. Tsuji, H. Shirai, Combust. Flame 159 (2012) 353–366.

[23] S. Niksa, A. Kerstein, Energy Fuels 5 (1991) 647–665.

[24] S.J. Brookes, J.B. Moss, Combust. Flame 116 (1999) 486-503.

[25] K.M. Leung, R.P. Lindstedt, W.P. Jones, Combust. Flame 87 (1991) 289–305.

[26] H. Breitbach, J. Goettgens, F. Mauss, H. Pitsch, N. Peters, Proc. Combust. Inst. 25 (1994) 1357–1364.

[27] G.D. Ulrich, Combust. Sci. Technol. 4 (1971) 47–57.

[28] J. Ma, T.H. Fletcher, B.W. Webb, Proc. Combust. Inst. 26 (1996) 3161–3167.

[29] K.B. Lee, M.W. Thring, J.M. Beér, Combust. Flame 6 (1962) 137–145.

[30] M. Fairweather, W.P. Jones, R.P. Lindstedt, Combust. Flame 89 (1992) 45–63.

[31] W.A. Fiveland, J. Heat Transfer 106 (1984) 699.

[32] R. Kurose, H. Makino, A. Suzuki, Fuel 83 (2004) 693–703.

[33] Z. Wen, S. Yun, M.J. Thomson, M.F. Lightstone, Combust. Flame 135 (2003) 323–340.

[34] M.A. Field, Combust. Flame 13 (1969) 237–252.

[35] D.E.S.C.T. Crowe, M.P. Sharma, Trans. ASME J. Fluids Eng. 99 (1977) 325–332.

[36] P.E. DesJardin, S.H. Frankel, Phys. Fluids 10 (1998) 2298.

[37] R. Kurose, H. Makino, T. Michioka, Combust. Flame 127 (2001) 2157–2163.